

# Quantitative Morphology of Galaxies from the SDSS I: Luminosity in Bulges and Disks

Lidia A.M. Tasca<sup>1\*</sup> and Simon D.M. White<sup>1</sup>

<sup>1</sup>*Max-Planck-Institut für Astrophysik, Karl-Schwarzschild-Str. 1 85741 Garching b. München, Germany*

16 November 2018

## ABSTRACT

In the first paper of this series we use the publicly available code **Gim2D** to model the  $r$ - and  $i$ -band images of all galaxies in a magnitude-limited sample of roughly 1800 morphologically classified galaxies taken from the Sloan Digital Sky Survey. The model is a concentric superposition of two components, each with elliptical isophotes with constant flattening and position angle. The disk luminosity profile is assumed exponential, while the bulge is assumed to have a de Vaucouleurs or a Sérsic profile. We find that the parameters returned by **Gim2D** depend little on the waveband or bulge profile used; their formal uncertainties are usually small. Nevertheless, for bright galaxies the measured distribution of  $b/a$ , the apparent disk flattening, deviates strongly from the expected uniform distribution, showing that the “disk” identified by the code frequently corresponds to an intrinsically 3-dimensional structure rather than to a true thin disk. We correct approximately for this systematic problem using the observed statistics of the  $b/a$  distribution and estimate, as a function of absolute magnitude, the mean fractions of galaxy light in disks and in “pure bulge” systems (those with no detectable disk). For the brightest galaxies the disk light fraction is about 10% and about 80% are “pure bulge” systems. For faint galaxies most of the light is in disks and we do not detect a “pure bulge” population. Averaging over the galaxy population as a whole, we find that  $54 \pm 2\%$  of the local cosmic luminosity density at both  $r$  and  $i$  comes from disks and  $32 \pm 2\%$  from “pure bulge” systems. The remaining  $14 \pm 2\%$  comes from bulges in galaxies with detectable disks.

**Key words:** Survey – galaxies: photometry – galaxies: bulge–to–disk decomposition – galaxies: fundamental parameters – galaxies: spirals – galaxies: ellipticals – galaxies: bulge – galaxies: disk

## 1 INTRODUCTION

Observations show that galaxies typically have two components with different photometric and dynamical properties: a thin, rotationally supported stellar disk which often also contains gas and dust, and a bulge, a spheroidal or ellipsoidal component made purely of stars. Most galaxies possess both structures, but some, the ellipticals, have no significant disk, while others, late-type spirals and irregulars, have little or no bulge. Since these two components presumably had different formation paths, their relative importance must be a fundamental clue to how each galaxy formed. Among the disk galaxies themselves there exists a dichotomy between those rich in gas, dust and the accompanying star formation, spiral and irregular galaxies, and those in which this activity is virtually absent, lenticular galaxies.

It is known that galaxies of differing morphology are

segregated according to environmental density (Dressler 1980) with the low-density field composed largely of spirals and irregulars and the densest regions of clusters composed of lenticulars and ellipticals. Many interpretations have been proposed for this observation, ranging from initial condition biases which imprint the differences at birth, to gravitational, gas dynamical or radiative processes through which galactic environment affects later evolution. Recent studies using the large, complete samples provided by the Sloan Digital Sky Survey (SDSS, see below) show the distribution of galaxy mass to depend quite strongly on environment, apparently reflecting an initial condition bias, while for galaxies of given mass, star formation properties depend much more strongly on environment than do structural properties, suggesting that external processes primarily affect the gas component from which stars form (Kauffmann et al. 2004).

Understanding the chronology of bulge and disk formation by analysing the relative contributions of these two components at different cosmological epochs is a fundamental

\* E-mail: lidia.tasca@oamp.fr

goal of observational cosmology. Such data provide important constraints on competing scenarios of galaxy formation and evolution. In models where bulges form first and disks are added later no close correlation is expected between the two formation phases; the ratio of spheroid luminosity to total luminosity measures the efficiency of the first burst of star formation relative to later slow accretion (Fall & Efstathiou 1980; Kauffmann, White & Guiderdoni 1993). If instead bulges form out of disks by secular evolution, then a stronger correlation between their properties may be expected (Norman et al. 1996; Bournaud & Combes 2004).

The relative contributions of bulges and disks to the stellar content of galaxies of differing mass and also to the overall stellar content of the Universe are clearly important quantities which should be reproduced within any viable picture of galaxy formation. It has long been known that the massive galaxy population is dominated by light from spheroids, while disks tend to dominate in lower mass populations (e.g. Efstathiou et al. (1982)), but there have been no recent quantitative studies for the galaxy population as a whole. The most commonly cited estimates of the fractions of all stars in bulges and disks trace back to the work of Simien & de Vaucouleurs (1986) and Schechter & Dressler (1987). These results suffer from poor statistics and are based largely on photographic material and on visual “decomposition” of the light of each galaxy into its bulge and disk fractions. With large photometric surveys, linear CCD detectors and quantitative decomposition techniques it should clearly be possible to do much better. This is the goal of the present paper and subsequent papers in this series.

We apply a modern two-dimensional morphological decomposition algorithm to the images of a magnitude-limited sample of relatively nearby and bright galaxies with photometry available from SDSS. In this paper we use the results to study the overall contribution of disks and bulges to the light of the nearby galaxy population both as a function of intrinsic galaxy luminosity and for the population as a whole. In section 2 we describe the selection of the sample we use. In section 3 we describe the decomposition algorithm and the parametric functions it uses to fit the galaxy images. We also describe how the data were processed. In section 4 results are compared for different photometric bands and for different parametric fitting functions in order to explore the robustness of the results. Deviations of the images from the best fit models are also quantified. In section 5 we study the distribution of derived parameters for those galaxies which could be successfully fitted. We also identify and correct for a serious (and previously known) systematic which results in the assignment of significant disks to bright galaxies where disks are in most cases actually absent. This section presents our principal results, estimates of the fractions of the total light of all galaxies of given luminosity which are in disks, in bulges, in galaxies with no detectable disk or in galaxies with no detectable bulge. Combining these with previous measurements of the galaxy luminosity function allows us to obtain corresponding fractions for the galaxy population as a whole. A final section discusses and summarises these results.

Throughout this paper, unless otherwise stated, we assume a Hubble constant of  $H_0 = 70 \text{ km s}^{-1} \text{ Mpc}^{-1}$  and an

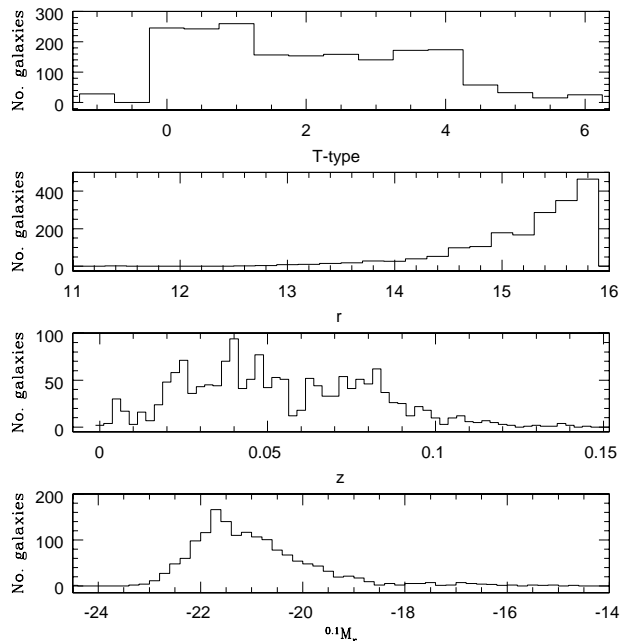


**Figure 1.** The distributions of galaxies in morphological type (upper panel) and in extinction-corrected Petrosian apparent magnitude in the  $r$  band (second panel) are shown for the 1862 galaxies in our sample. The redshift (third panel) and corresponding absolute magnitude (lower panel) distributions are given for the 1550 galaxies in the sample for which we have spectroscopic information.

$\Omega_M = 0.3$ ,  $\Omega_\Lambda = 0.7$  cosmology in calculating distances and luminosities.

## 2 OBSERVATIONAL DATA

### 2.1 Galaxy sample

In June 2001 the Sloan Digital Sky Survey (SDSS; York et al. (2000)) released its Early Data Release (EDR; Stoughton et al. (2002)), roughly 462 square degrees of imaging data collected in drift scan mode. The imaging is conducted in the  $u$ -,  $g$ -,  $r$ -,  $i$ - and  $z$ -bands (Fukugita et al. (1996); Gunn et al. (1998); Hogg et al. (2001); Smith et al. (2002); Pier et al. (2003)). The reader is referred to Ivezić et al. (2004) for details on the photometric quality assessment. The EDR contains around a million galaxies distributed within a narrow strip of 2.5 degrees across the equator. As the strip crosses the galactic plane, the data are divided into two separate sets in the North and South Galactic caps. The SDSS has the ambitious goal to image a quarter of the Celestial Sphere at high Galactic latitude as well as to obtain spectra uniformly for all the brighter galaxies. For the present project this has the advantage, in comparison to previous work, of having uniform photometry and spectroscopy over a much larger area, permitting a major improvement in sample size and homogeneity.

In the following analysis we are using a sample of

| Sample        | Subsamples          |                      |                      |                      |                      |                      |                |                          | Total |
|---------------|---------------------|----------------------|----------------------|----------------------|----------------------|----------------------|----------------|--------------------------|-------|
|               | $0 \leq T < 1$<br>E | $1 \leq T < 2$<br>S0 | $2 \leq T < 3$<br>Sa | $3 \leq T < 4$<br>Sb | $4 \leq T < 5$<br>Sc | $5 \leq T < 6$<br>Sd | $T = 6$<br>Irr | $T = -1$<br>unclassified |       |
| Photometric   | 487                 | 417                  | 313                  | 312                  | 232                  | 48                   | 25             | 28                       | 1862  |
| Spectroscopic | 413                 | 363                  | 272                  | 262                  | 197                  | 42                   | 16             | 23                       | 1588  |

**Table 1.** Visual classification of our photometric and spectroscopic samples into morphological subsamples.

galaxies defined by the Japanese Participation Group (JPG, Nakamura et al. (2003)). This is a homogeneous sample obtained from the northern equatorial stripes of the SDSS EDR. The region of the sky covered is an area of 229.7 square degrees at  $145.15^\circ \leq \alpha \leq 235.97^\circ$  and  $-1.27^\circ \leq \delta \leq 1.27^\circ$ . The sample is limited to bright galaxies with  $r \leq 15.9$  after Galactic reddening correction. Eye classifications cannot be made confidently beyond this magnitude, and for our current purpose this bright limit has the advantage that the galaxies are all large compared to the SDSS point-spread function.

All the 1862 galaxies in the sample were classified by eye on the system of the *Hubble Atlas of Galaxies* (Sandage 1961) by JPG scientists using the  $g$  band image of each galaxy. For each galaxy the final quoted type is the mean of 4 independent classifications by different scientists. The *rms* of these 4 classifications is also given; they typically agree within  $\Delta T \leq 1.5$ . The corresponding numerical classification as defined in the *Third Reference Catalogue of Bright Galaxies* (de Vaucouleurs et al. 1991) is also reported. The seven resulting subsamples separate galaxies according to morphology going from ellipticals (E) through lenticulars (S0) and early-type spirals (Sa, Sb), to late-type spirals (Sc, Sd) and irregulars (Irr). For 1588 galaxies out of our sample of 1862 we have spectroscopic information. A summary of the distribution of our galaxies across the morphological classes is given in Table 1. We refer to (Nakamura et al. 2003) for further details. Further work exploring the properties of this sample can be found in Nakamura et al. (2004), Kelly & McKay (2004) and Fukugita et al. (2004).

## 2.2 Photometric and spectroscopic data

Two important quantities used in this paper are taken directly from the SDSS database: the redshift and the Petrosian magnitude. The first is obtained by the spectroscopic pipelines **idllspec2d** (written by D.Schlegel & S.Burles) and **spectro1d** (written by M. SubbaRao, M. Bernardi and J. Frieman). A description of the tiling algorithm used to assign targets to each pointing is given in Blanton et al. (2003). The SDSS spectroscopic galaxy samples consist of all galaxies brighter than  $r = 17.77$  (Strauss et al. 2002) and of a sample of luminous red galaxies (Eisenstein et al. 2001) extending at  $r < 19.2$ . The distribution of galaxies with respect to  $z$  for our sample is shown in the third panel of Figure 1. The second quantity is obtained by the **Photo** pipeline (see Lupton et al. (2001, 2002)) and it is based on a modified form of the Petrosian system for galaxy photometry which is designed to measure a constant (and large) fraction of the total light of a galaxy independent of its characteristic surface brightness. Three related quantities also used in this paper are  $R_{50}$  and  $R_{90}$ , defined as the radii which include respectively 50 and 90 percent of the Petrosian flux in the  $r$  band (see Stoughton et al. (2002)), and the concentration index

$c \equiv R_{90}/R_{50}$ . The second panel of Figure 1 shows the distribution of galaxies with respect to their Petrosian magnitude after correction for foreground Galactic extinction using the reddening map of Schlegel et al. (1998). Such extinction-corrected Petrosian magnitudes are used throughout this paper.

## 3 IMAGE ANALYSIS

### 3.1 The fitting algorithm

We examine the structural properties of our galaxies using **Gim2D** (Simard et al. 2002), a two-dimensional photometric decomposition algorithm which fits each image to a superposition of an elliptical component with a Sérsic profile, representing the bulge, and a concentric elliptical component with an exponential profile, representing the disk. It is important to recognise that this separation into bulge and disk is based only on the observed image, and may not correspond to the “best” decomposition if additional information, for example from kinematics of the stars or the gas, is taken into account.

It is well known that the bulge component of most galaxies can be well represented by a surface brightness profile of Sérsic form:

$$\Sigma(r) = \Sigma_e \cdot \exp \{-b[(r/r_e)^{1/n} - 1]\} \quad (1)$$

where  $\Sigma(r)$  is the surface brightness a distance  $r$  from the centre along the semi-major axis and  $\Sigma_e$  is its characteristic value, the effective surface brightness, defined as the value at the effective radius  $r_e$ . The parameter  $b$  is related to the Sérsic index  $n$  and is set equal to  $1.9992n - 0.3271$  so that  $r_e$  is the projected radius enclosing half of the total light (Sérsic 1968; Ciotti 1991). Many authors fit bulges and ellipticals with a more specific function, the de Vaucouleurs  $r^{1/4}$  law, which is obtained by setting  $n = 4$ . When fitting Sérsic profiles in the following we will assume  $0.2 < n < 4$ . This choice is driven by the knowledge that fits to low-luminosity ellipticals and bulges generally give  $n$  significantly smaller than 4, the standard value for bright ellipticals (de Jong 1996; Caon et al. 2005). Values of  $n$  in excess of 4 are sometimes found for cD galaxies but our sample does not contain such exceptionally luminous systems.

Disks are generally well described by an exponential profile (corresponding to  $n = 1$ ), although non-axisymmetric features due to bars, spiral arms and dust lanes can be large. We use the standard parametrisation:

$$\Sigma(r) = \Sigma_0 \cdot \exp(-r/h) , \quad (2)$$

where  $\Sigma_0$  is the central surface brightness and  $h$  the disk scalelength.

These laws are purely empirical fitting functions with no

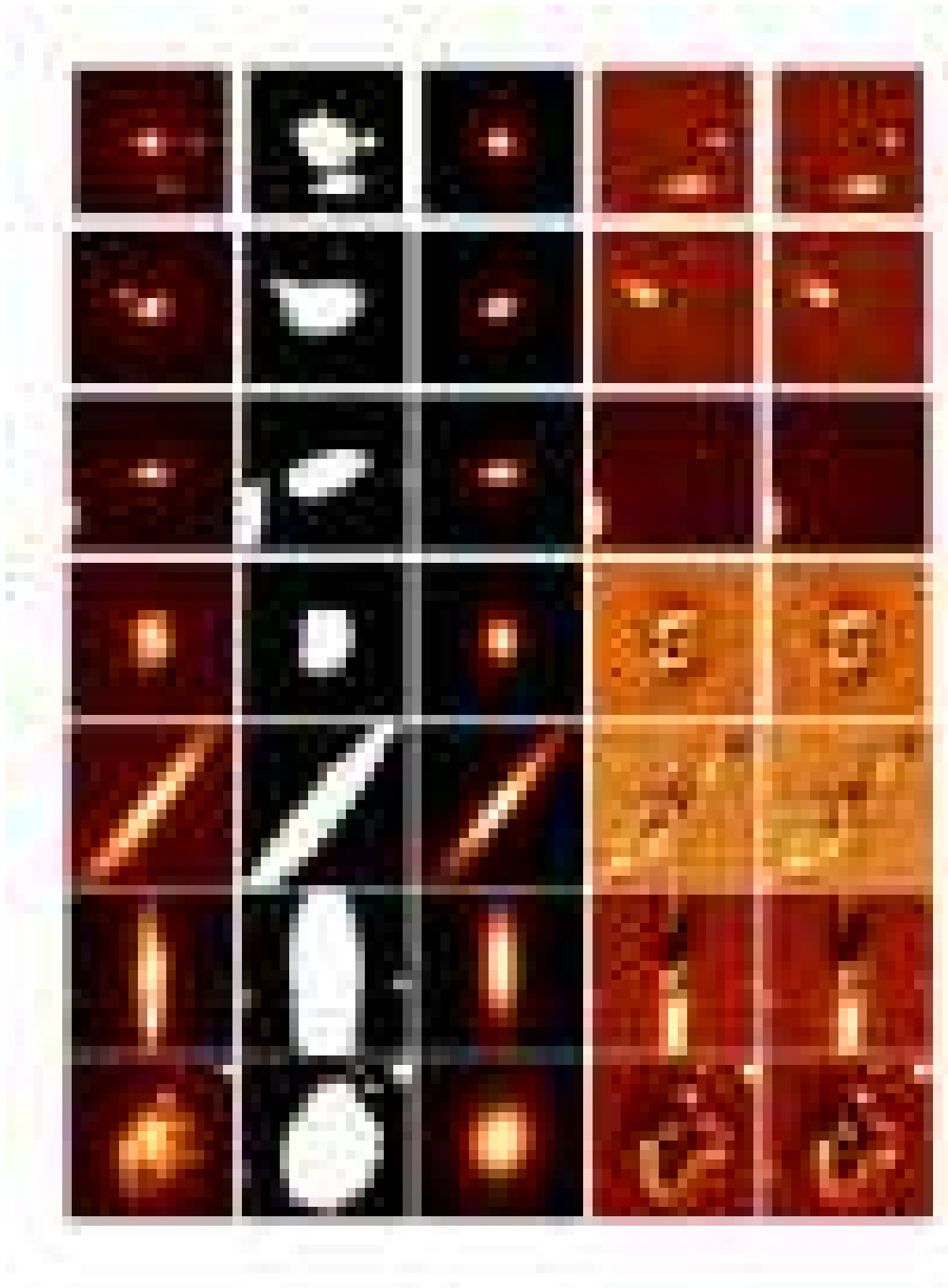


**Figure 2.** Examples of the science image, the mask, the model and the residual images for our two fits (de Vaucouleurs plus exponential or Sérsic plus exponential) in the  $r$  band (from left to right) for galaxies from our seven morphological classes: E, S0, Sa, Sb, Sc, Sd, Irr (from top to bottom).

strong theoretical justification. Other functions might provide equally good fits to a galaxy profile leading to a different parametrisation for the bulge–to–disk decomposition, and possibly different values for global parameters such as the bulge-to-total luminosity ratio  $B/T$ .

With this model there is a maximum of twelve parameters which are adjusted in fitting the galaxy image and that we retrieve as output from our decomposition: the total flux of the object; the bulge–to–total light ratio  $B/T$ , defined as the fraction of the total flux in the bulge component so that  $B/T = 1$  corresponds to a pure bulge and  $B/T = 0$  to a pure disk; the bulge effective radius  $r_e$ ; the disk scalelength  $h$ ; the disk inclination angle  $i$  defined so that  $i = 0$  for face-on disks and  $i = 90$  for edge-on ones – the disk axial ratio is then  $(b/a)_{disk} = \cos(i)$ ; the bulge ellipticity  $e$  given in terms of the bulge axial ratio by  $e = 1 - (b/a)$ ; the bulge and disk position angles (hereafter PA) measured clockwise from north and allowed to be different; the Sérsic index  $n$  which we sometimes fix at  $n = 4$ ; the x-y pixel shifts  $dx$  and  $dy$  of the galaxy centre position in the model and science thumbnail images; and the background intensity level.

Additional parameters could be introduced to model other features (e.g bars, spiral arms, etc.) but such decompositions become somewhat arbitrary and may not converge to unique solutions. Our current choice is standard and we found it to be a good compromise between stability of results and flexibility of representation. Notice that for an axisymmetric galaxy the position angles of the bulge and the disk would be the same. Allowing them to differ makes it possible for the code to detect triaxial bulges or bars in suitably oriented galaxies.

### 3.2 Image reduction

We perform our analysis starting from corrected frames of area  $13'.52 \times 8'.98$  taken directly from the SDSS archive. In these large-scale images flat-field, bias, cosmic-ray, and pixel-defect corrections have already been applied. The pixel-size in these images is 0,396 arcsec. To proceed with our fitting, we begin with a list of source positions and apply the **SExtractor** galaxy photometry package version 2.2.2 (Bertin & Arnouts 1996) to each field to estimate the local sky background level at each point and to define the isophotal area where each object is above the detection threshold (we choose a threshold which is higher than background by 1.5 times the background noise). When SExtractor performs galaxy photometry, it constructs a segmentation (or mask) image in which pixels belonging to the same object all have the same value and sky background pixels are flagged by zeros. Our 2-D image fit is carried out on all pixels belonging to the same SExtractor-defined object. In practice **Gim2D** uses thumbnail images, two for each galaxy, extracted around the object of interest. The area of these is chosen to be 10 times larger than the mask area defined by SExtractor. The first thumbnail is cut from the corrected frame and is corrected for the local background estimated by SExtractor, while the second contains the corresponding pixels from the mask image. The fit then produces values and uncertainty ranges for each model parameter. Subtraction of the best-fit model from the input thumbnail produces a residual image that can be used to characterise how well the model fits the galaxy. Examples of all these images

for representative galaxies from each of our morphological classes are shown in Figure 2.

When the fitting algorithm starts to sample the 12-dimensional parameter space, it considers not only the pixels assigned to the main galaxy by the mask but all pixels flagged as object or background in the SExtractor segmentation image. Important information about the galaxy could be contained in the pixels below the detection threshold. In the residual images (see Figure 2) one can see that all pixels belonging to other objects in the vicinity of the one under consideration are masked out. The final flux is obtained by the integration of the best fit model over all pixels, assuring that we do not lose the flux in the masked regions.

The model image of each galaxy is convolved with a point spread function (PSF) before comparison with the real data. The PSF can be highly variable across a corrected frame (Stoughton et al. 2002) and for this reason it is important to interpolate the PSF parameters measured for individual stars to the position of each galaxy before convolving with the model. Our galaxy light model is thus the sum of an exponential disk and a Sérsic, or de Vaucouleurs, bulge, convolved with this “best” PSF.

Finally a photometric calibration and the redshift are required to retrieve physical quantities from the output of the B/D decomposition code.

## 4 ARE WE CONFIDENT OF OUR DECOMPOSITIONS?

We have carried out the above fitting procedure entirely independently for each of our galaxies in the  $r$  and the  $i$  bands. The two segmentation images differ slightly and in addition there are colour variations across many of our galaxies as a result of variations in the underlying stellar populations and in the dust distribution. It is thus reassuring that the structural parameters in the two bands are in good agreement in the great majority of cases (see below). This shows that the fitting procedure produces stable results. In addition **Gim2D** produces acceptable converged parameter sets for almost all the galaxies in both bands. In Table 2 we show the number of galaxies from our spectroscopic sample that are successfully modelled by the code in each band in the two cases when the Sérsic index is set equal to 4 and when it is allowed to float. We consider a fit to be successful when the code is converging. As expected slightly more galaxies can be fit when  $n$  is kept free, and in this case only  $\sim 50$  of our 1834 galaxies cannot be fit acceptably in either of the two bands. These galaxies are almost all later type spirals (Sb–Sc–Sd) which are not modelled simply because the centroid position provided by the SDSS database does not match the one obtained with SExtractor within the defined 4 arcsec searching radius. It is interesting to notice that the modelling also fails occasionally for early-type objects when these are forced to follow a de Vaucouleurs law for the central photometric component. We now discuss aspects of these fits in more detail.

### 4.1 Comparison between fits

As already noted, we have fitted all our galaxies with a bulge model in which the Sérsic index  $n$  is free and also with a

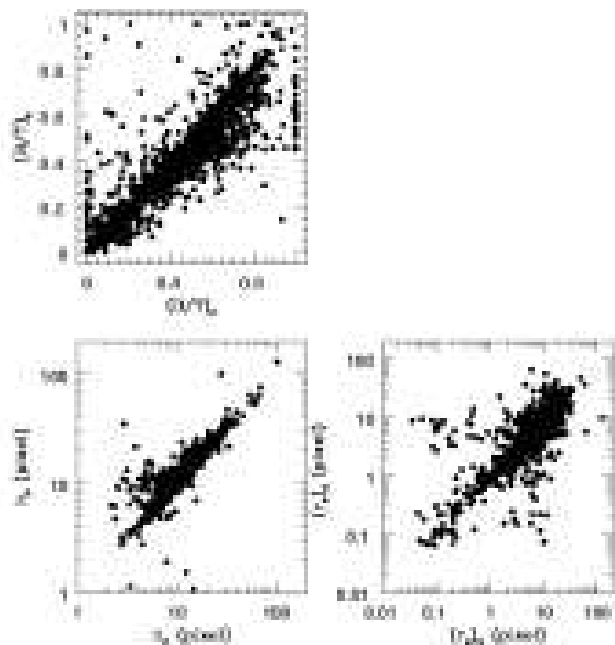


**Figure 3.** The bulge fraction (upper-left), the disk scalelength (lower-left) and the effective radius of the bulge (lower-right) obtained using different parametric functions to perform the decomposition (de Vaucouleurs plus exponential on the x-axis and Sérsic plus exponential on the y-axis) are plotted against each other for 1702 galaxies in the  $i$  band.

model in which it is fixed to the de Vaucouleurs value  $n = 4$ . In this subsection we show that the parameters of the decomposition of most interest to us are only weakly affected by this choice for most galaxies. In Figure 3 we compare the values of the bulge fraction  $B/T$ , of the disk scale length  $h$  and of the bulge effective radius  $r_e$  obtained for each galaxy in the two cases. We show results for the  $r$  band only (results for  $i$  are similar).

#### 4.2 Comparison between different bands

In this section we compare the parameters estimated for each galaxy when the same model is fit independently to images in each of the two SDSS bands analysed here. In Figures 4 and 5 we plot the retrieved parameters in the Sloan  $i$  and  $r$  bands against each other for the 1636 galaxies modelled successfully in both bands assuming a de Vaucouleurs profile for the bulge and an exponential for the disk. The corresponding results are shown in Figure 6 and 7 for the 1766 galaxies modelled successfully in both bands assuming a Sérsic profile for the bulge and an exponential for the disk; in this case, however, we also compare the values of the index  $n$  found in the two cases.

In the apparent magnitude plot there are only few isolated points while the rest correlate very well, the scatter being consistent with the expected variation in mean colour. The scatter in bulge-to-total light ratio is also gratifyingly small for the vast majority of the galaxies, particularly when  $n$  is fixed to the de Vaucouleurs value. The scatter is slightly

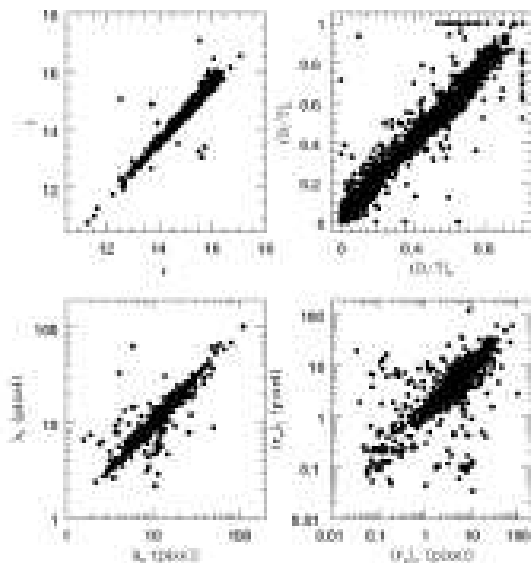


**Figure 4.** The total flux (upper-left), the bulge fraction (upper-right), the disk scalelength (lower-left) and the effective radius of the bulge (lower-right) in the  $i$  and  $r$  bands are plotted against each other for the 1638 galaxies modelled in both bands by fitting a de Vaucouleurs profile to the bulge and an exponential to the disk.

larger when  $n$  floats because different best fit values of the index in the two bands (see Figure 7) lead to different splits of the luminosity between bulge and disk. In most cases, however, similar  $n$  values are found in the two bands. The “arrow” shape of the  $B/T$  plots reflects the fact that the data in one band occasionally prefer a weak disk while no disk is present in the best fit in the other band.

There is also quite good agreement between the values of the scalelengths for the bulge and disk components measured in the two bands. The agreement is worse for bulges than for disks and for components of small angular size compared to larger ones. This is presumably a reflection of resolution problems due to the finite pixel size and to difficulties with the PSF deconvolution. Nevertheless the apparent axial ratios of both bulges and disks agree well in the two bands with the scatter increasing for rounder systems. The agreement between the position angle of the disk in the considered photometric bands is pretty good even if a substantial scatter is present. The points in the two extreme corners could be moved by a simple rotation of  $180^\circ$ . In addition we check that the distribution of the position angle is consistent with a random orientation on the sky.

#### 4.3 Error estimates and goodness of fit

When carrying out its fitting **Gim2D** constructs a  $\chi^2$  value for each PSF-convolved model by summing over all pixels within the mask the square of the difference between model and data divided by the variance of the pixel noise, assumed to be due entirely to photon statistics. This measure of goodness of fit is then minimised over all parameters (each required to lie within a prespecified “allowed” range) to lo-

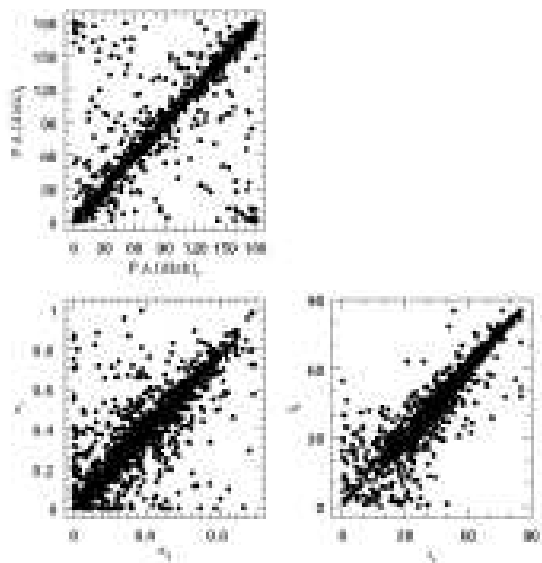


**Figure 5.** The position angle of the disk (upper-left), the ellipticity of the bulge (lower-left) and the inclination angle of the disk (lower-right) in the  $i$  and  $r$  bands are plotted against each other for the 1638 galaxies modelled in both bands by fitting a de Vaucouleurs profile to the bulge and an exponential to the disk.

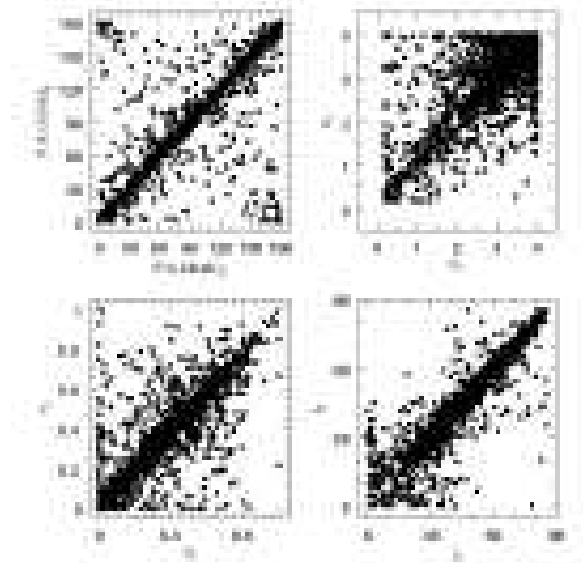


**Figure 7.** Similar to Figure 5 but for the 1766 galaxies modelled in both bands by fitting a Sérsic profile to the bulge and an exponential to the disk. In this figure we also compare the values of the Sérsic index  $n$  found in the two bands (upper right).

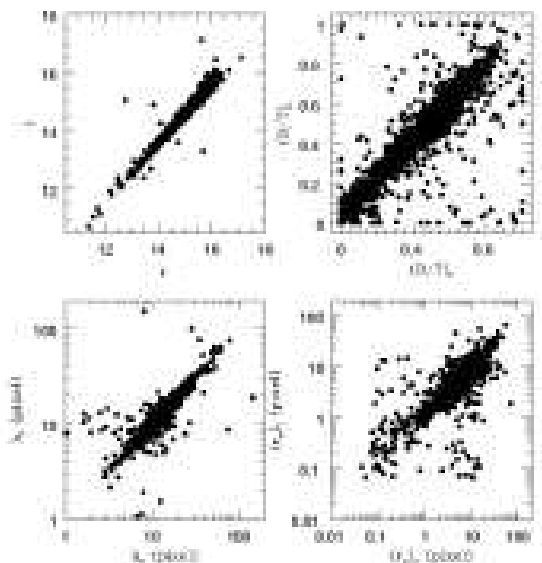


**Figure 6.** The same as Figure 4 but for the 1766 galaxies modelled in both bands by fitting a Sérsic profile to the bulge and an exponential to the disk.

cate the maximum likelihood model. Once the algorithm has converged, the region of parameter space surrounding the likelihood maximum is sampled in order to compute marginalised *a posteriori* one-dimensional probability distributions for each model parameter. These are then used to define best parameter estimates, taken to be the medians

of these distributions, and 99% confidence ranges defined by their upper and lower 0.5% points. Nevertheless he computed  $\chi^2$  turns out to be not too sensitive to whether problems occur in the decomposition (i.e. a wrong point spread function) or the decomposition reliably describes the light distribution in the galaxy.

With the aim of better understanding the goodness of the fit of our models we introduce two additional measures,  $G_1$  and  $G_2$ , which characterise the size of the residuals without reference either to the overall luminosity and size scales of a galaxy or to the expected counting noise. They are defined using the region flagged as belonging to the galaxy in the segmentation image generated by SExtractor.  $G_1$  is the difference between the model and observed luminosities in this region as a fraction of the model luminosity, while  $G_2$  is the ratio of the sum of the absolute values of the residuals in all the pixels to the model luminosity. Working from the individual pixels ( $ij$ ), by definition the total counts in the science image ( $\sum O_{ij}$ ) and in the model image ( $\sum M_{ij}$ ) are due to the light of the galaxy plus a uniform sky ( $\sum S_{ij}$ ), which is the same in the two images. The total counts in the residual image simply reflect the difference between the luminosity of the observed and modelled galaxy ( $\sum D_{ij} = \sum O_{ij} - \sum M_{ij}$ ). Our definitions can consequently be formulated as:

$$G_1 = \frac{\sum D_{ij}}{L_{model}} \quad \text{and} \quad G_2 = \frac{\sum |D_{ij}|}{L_{model}} \quad (3)$$

Figure 8 shows the distribution of galaxies with respect to these quantities as a function of galaxy absolute magnitude. Results are presented for fits to the  $i$  band data both for floating  $n$  and for  $n$  fixed to the de Vaucouleurs value. Results for the  $r$  band are very similar. The  $G_1$  parameter is

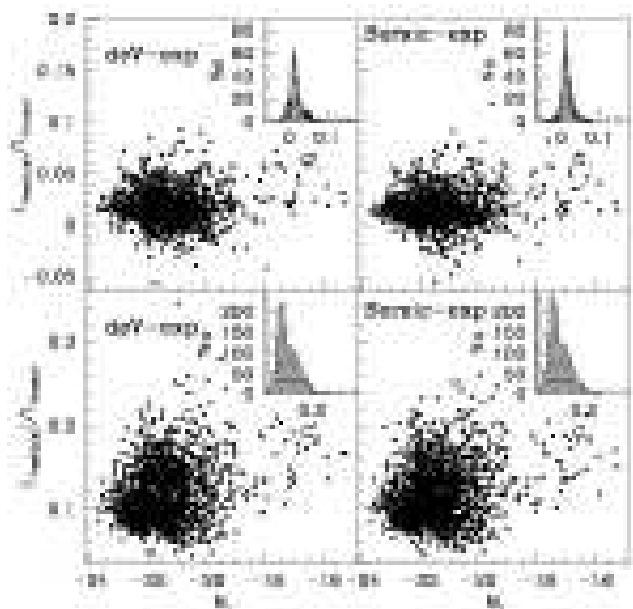


**Figure 8.** Goodness of fit measures for our two-component modelling of the  $i$ -band images. The two left-hand panels give results for the 1469 galaxies modelled successfully using a de Vaucouleurs profile for the bulge and an exponential profile for the disk. The two right-hand panels give results for the 1532 galaxies modelled successfully when we use the more general Sérsic profile for the bulge. The two upper panels show results for  $G_1$ , the total light in the residual image in units of the total light of the model. The two lower panels give results for  $G_2$ , the sum of the absolute values of the individual pixel deviations from the model again in units of the total model luminosity.  $G_1$  and  $G_2$  are plotted against absolute magnitude in the main part of each panel while a histogram of their marginal distribution is given in the inset.

narrowly distributed around zero, with a slight bias towards positive values. Thus **Gim2D** underestimates slightly the luminosities of these large galaxies, but typically by only a couple of percent. Misestimates by more than 5% are very rare. The distribution of  $G_2$  peaks at 0.1 and is skew with a longer tail towards higher values. There is a tendency for deviations from the models to be larger for intrinsically fainter galaxies, particularly below about  $M_i = -20$ . Residuals are only slightly reduced by the extra freedom involved in allowing  $n$  to vary because, as can be seen from the examples in Figure 2, the dominant residuals are often due to non-symmetric features such as spiral arms or dust lanes. We are encouraged that  $G_2$  is less than 15% for about three quarters of our galaxies and almost never rises as high as 25%. We therefore believe that our model represents the images of the majority of galaxies adequately for our purpose, and that derived parameters can be used meaningfully to characterise physical properties of the galaxies themselves.

## 5 RESULTS

### 5.1 Comparison of Sérsic index distributions

Previous studies (Andredakis 1998; Courteau et al. 1996; de Jong 1996) have shown that the Sérsic formula can fit the light profiles of many nearby ellipticals and bulges extremely

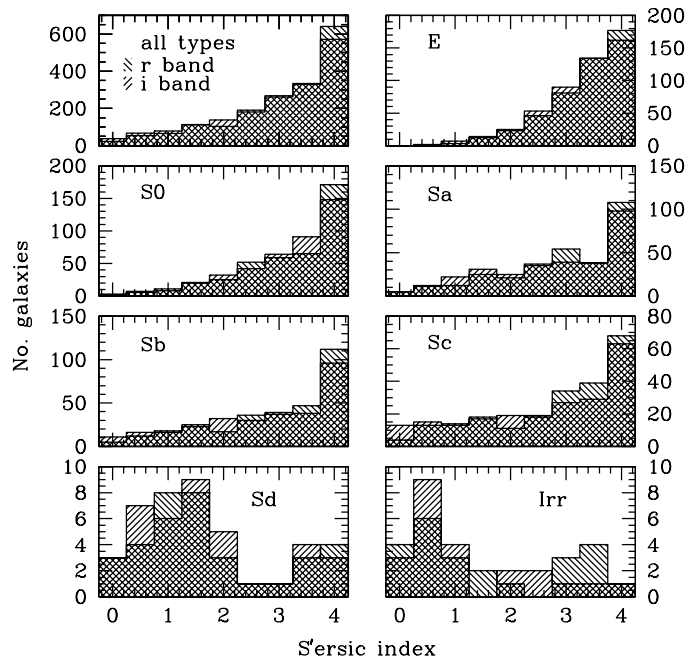


**Figure 9.** Distribution of the Sérsic index  $n$ . The upper-left panel shows the distribution for the total sample of 1790 and 1782 galaxies successfully modelled in the  $i$  and  $r$  band respectively. In the other panels the Sérsic index distribution is separated according to morphological type.

well. While massive systems usually require large values of  $n$ , similar to the de Vaucouleurs value, less massive ellipticals and bulges, particularly the bulges of late-type spirals usually demand smaller  $n$  values and indeed can often be well fit by an exponential law with  $n = 1$ . For our JPG sample when we allow the Sérsic index to assume any value between 0.2 and 4 we obtain the distributions shown in Figure 9. The upper-left histograms give results for the 1790 galaxies in the  $i$  band and the 1782 galaxies in the  $r$  band (out of the total sample of 1862) which are successfully fit by **Gim2D**. These distributions peak at  $n = 4$ , confirming that the  $r^{1/4}$  law provides an acceptable fit to the bulge component of a large fraction of the galaxies in a magnitude-limited sample. In the other panels of Figure 9 we split the sample by morphological type and it becomes evident that most E/S0 galaxies are well described by values of  $n$  close to than 4. The same is true for the bulges of most early-type spirals. For later-type spirals there is a clear shift to lower values of  $n$ . for many of these objects  $n \sim 1$  is preferred, confirming the earlier studies referred to above. Note that the distributions in Figure 9 are almost independent of the band in which the decomposition is carried out, confirming the robustness of the results.

### 5.2 Disk and Bulge luminosity

In this section we derive the fraction of the luminosity density in the local universe in bulges and in disks for the Sloan  $i$  and  $r$  bands, starting from our complete sample of  $r$ -selected galaxies with  $r < 15.9$  (after correction for Galactic extinc-

| Galaxies modelled            |               |               |
|------------------------------|---------------|---------------|
| Type of fit                  | <i>r</i> band | <i>i</i> band |
| de Vaucouleurs + exponential | 1450          | 1469          |
| Sérsic + exponential         | 1528          | 1532          |

**Table 2.** Galaxies in the spectroscopic sample that we use to calculate the fraction of light in the local universe in disks and bulges. Of the 1588 galaxies in our sample for which the redshift is known, 1517 are successfully modelled by the code in both bands when using the Sérsic profile and 1409 if we adopt the de Vaucouleurs law. In the table we show the number of galaxies in the *i* and *r* bands for which we have the spectroscopy, the decomposition parameters and good photometry.

| Type of fit                  | <i>r</i> band        | <i>i</i> band        |
|------------------------------|----------------------|----------------------|
| de Vaucouleurs + exponential | $(58.92 \pm 2.40)\%$ | $(54.92 \pm 2.02)\%$ |
| Sérsic + exponential         | $(54.82 \pm 1.95)\%$ | $(55.41 \pm 1.98)\%$ |

**Table 3.** Total fraction of the light in disks in the local universe in the *r* and *i* bands and for fits requiring  $n = 4$  and allowing  $n$  to vary over  $0.2 \leq n \leq 4$ .

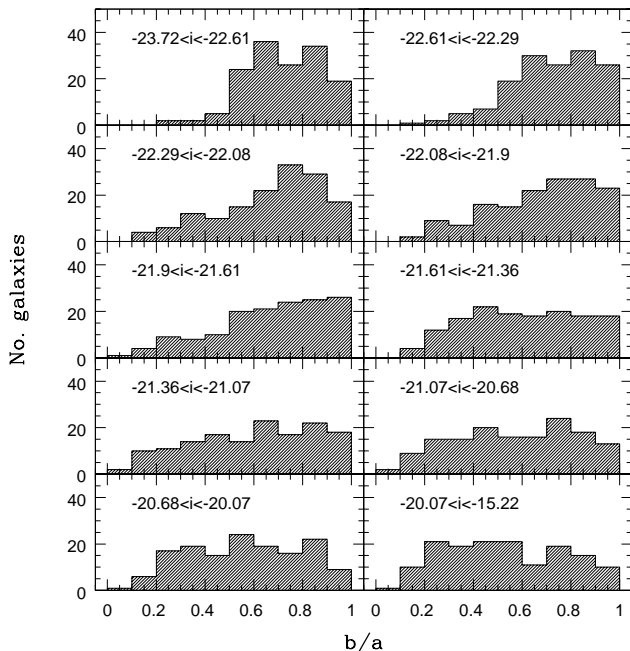


**Figure 10.** Distribution of apparent axial ratio for the disk components of the 1469 galaxies with a redshift which were modelled successfully in the *i* band by a de Vaucouleurs plus an exponential. Galaxies are split by absolute magnitude into 10 bins containing approximately equal numbers of objects.

tion). From our total sample of 1862 galaxies we here consider only the 1588 objects for which spectroscopic data are available and it is therefore possible to measure the absolute magnitudes needed by our estimation procedure. The absolute magnitudes used in this paper are *k*-corrected using the code of Blanton et al. (2003), *v2\_16*. In the SDSS main galaxy sample as a whole the median redshift is near  $z = 0.1$ , so Blanton chose to express results in the SDSS filter system shifted by 0.1. For our sample the median redshift is about 0.05. Nevertheless for consistency with other SDSS work (in particular, with the luminosity functions we use below) we follow Blanton’s convention and *k*-correct to  $z = 0.1$ . We denote absolute magnitudes in this system as

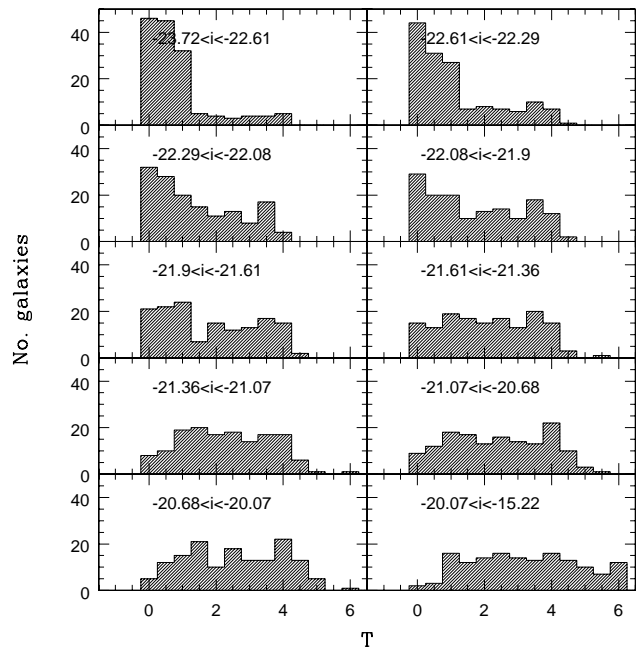


**Figure 11.** As Figure 10 but showing the distribution over morphological type.

$^{0.1}M_r$  and  $^{0.1}M_i$  to distinguish them those in the unshifted system. Since our primary results concern the *ratios* of luminosities in different components, this choice has no effect on our analysis

There are 23 objects in this set for which no morphological type was assigned by the JPG astronomers. We exclude these from further consideration here, leaving 1565 objects with redshift and a well defined “by eye” morphological type. From this sample we also excluded all galaxies for which **Gim2D** failed in the modelling, and in addition we removed three objects for which the *k*-correction is not reliable due to bad photometric data in the bluest and reddest bands. This reduced the number of objects used to estimate the luminosity densities in bulges and disks to the numbers in Table 2.

Our strategy for computing the fraction of the local lu-

| Type of fit                  | <i>r</i> band        | <i>i</i> band        |
|------------------------------|----------------------|----------------------|
| de Vaucouleurs + exponential | $(33.40 \pm 0.75)\%$ | $(31.15 \pm 0.73)\%$ |
| Sérsic + exponential         | $(34.39 \pm 0.72)\%$ | $(35.82 \pm 0.74)\%$ |

**Table 4.** Total fraction of the light in pure bulge systems in the local universe in the *r* and *i* bands and for fits requiring  $n = 4$  and allowing  $n$  to vary over  $0.2 \leq n \leq 4$ .

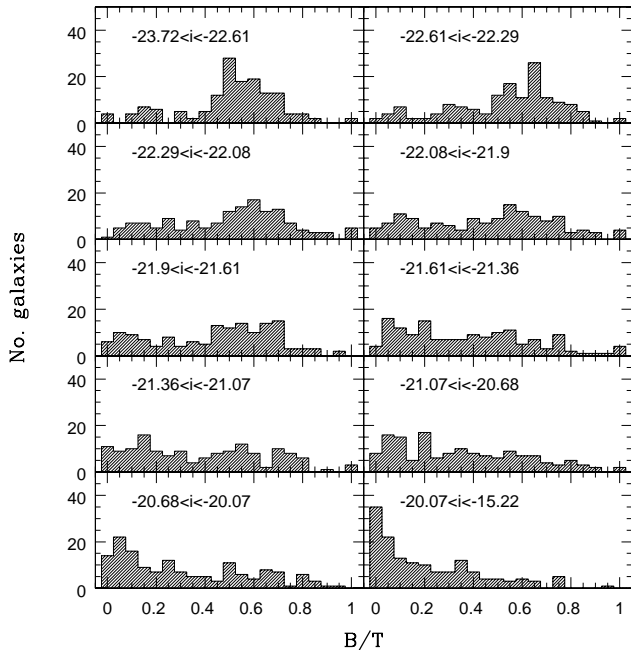


**Figure 12.** As Figure 10 but showing the distribution over bulge-to-disk ratio.

luminosity density which is in bulges and disks is as follows. We separate the galaxies in our sample into 11 bins according to their absolute luminosities in the *r* or *i* bands. The nine brightest bins each contain about 10% of the sample while the two faintest bins contain about 5% (we made this choice in order to get better luminosity coverage for faint galaxies.) For each bin we then use our decompositions to estimate the fraction of the total light coming from disks for galaxies at that absolute magnitude. Assuming this fraction to be appropriate for all galaxies of similar intrinsic brightness, we combine it with luminosity functions determined from much larger SDSS samples by Blanton et al. (2003) to obtain the fraction of the local luminosity density which is in disks. The complementary fraction is then the amount in bulges.

While this appears straightforward, a serious complication arises from the fact that 2-D fitting codes like **Gim2D** tend to fit radial variations in axial ratio or position angle in ellipsoidal galaxies by assigning a fraction of their light to a disk, when in fact none is present. This systematic is well known and is commented on in Simard et al. (2002). We can demonstrate its presence in our purely luminosity-selected data by examining the distribution of disk apparent axial ratio returned by **Gim2D**. The distribution of  $b/a$  is expected to be uniform on  $[0, 1]$  for randomly oriented thin disks. Figure 10 shows the distributions we actually obtain

for the “disks” in our sample, split into 10 equal bins by absolute total *i*-magnitude. While for faint galaxies these distributions are indeed consistent with being flat, in the brighter bins there is clearly a strong bias towards high  $b/a$ . Among the brightest galaxies almost no “disks” are found with  $b/a < 0.5$ . Figure 11 shows that these bright bins are dominated by early-type disks according to the visual classifications of the JPG. The absence of small  $b/a$  values demonstrates that few of these systems actually have significant thin disks, despite the fact that **Gim2D** assigns most of them  $B/T$  ratios substantially smaller than unity (see Figure 12).

In order to circumvent this problem in the following analysis we use only the galaxies in each absolute magnitude bin which have  $b/a < 0.5$ . We believe the great majority of these must be true disks since ellipticals with apparent axial ratios smaller than 0.5 are very rare. For random orientation the total number of true disks expected in the bin is just twice the number with  $b/a < 0.5$ . The total light in disks in the bin is, however, more than twice the light in the disks with  $b/a < 0.5$ , since dust extinction is significantly stronger in edge-on than in face-on disks. This must be corrected if we wish to obtain an unbiased estimate of the luminosity density in disks.

In practice, our procedure works as follows. For each absolute magnitude bin  $k$  we estimate the fraction of the light in the disk component as

$$f_{disk,k} = \frac{L_{disk,k}}{L_{tot,k}} \quad (4)$$

where  $L_{disk,k}$  is the total luminosity of the disks of the galaxies in the bin and  $L_{tot,k}$  is the total luminosity from all components of these same galaxies. Since we assume that we can rely on our decomposition only for edge-on systems, we split the numerator into two parts

$$f_{disk,k} = \frac{L_{b/a < 0.5, disk, k} + L_{b/a > 0.5, disk, k}}{L_{tot,k}} \quad (5)$$

where  $L_{b/a < 0.5, disk, k}$  is the luminosity due to “edge-on” disks with  $b/a < 0.5$  and is obtained directly from our decompositions. We estimate the luminosity  $L_{b/a > 0.5, disk, k}$  in “face-on” disks by assuming that true disks are randomly oriented and that their internal extinction  $A_\lambda$  depends on inclination according to the standard prescription

$$A_\lambda = \gamma_\lambda \log(a/b). \quad (6)$$

Here  $A_\lambda$  is the correction to exactly face-on orientation. Assuming this formula, it is a simple matter to relate the total luminosity density in disks to that in disks with  $b/a < 0.5$ . We find

$$L_{disk,k} = 2^{1+0.4\gamma_\lambda} \cdot L_{b/a < 0.5, disk, k}, \quad (7)$$

hence

$$f_{disk,k} = 2^{1+0.4\gamma_\lambda} \cdot \frac{L_{b/a < 0.5, disk, k}}{L_{tot,k}}. \quad (8)$$

The bulge to total ratio  $B/T$  is one of the structural parameters returned by **Gim2D** for each galaxy. In combination with the total absolute Petrosian magnitude (taken directly from the SDSS database) it allows us to estimate the disk luminosity of each object contributing to  $L_{b/a < 0.5, disk, k}$ . We obtain  $L_{tot, k}$  simply by summing the Petrosian luminosities of all galaxies in the bin regardless of their  $b/a$ . We take values for  $\gamma_\lambda$  from the work of Tully et al. (1998). Since the numerical coefficient on the right hand side of equation 8 is only slightly smaller at  $i$  than at  $r$  band, we assume the value 2.56 for both photometric bands.

The results of these calculations are shown in Figure 13 for the galaxies modelled successfully in the  $i$  and  $r$  bands. In each figure we show results separately for decompositions which force a de Vaucouleurs bulge and for decompositions in which we allow  $0.2 < n < 4$ . The pattern is very similar in all cases. The average light fraction in disks varies smoothly from about 10% in the brightest galaxies to almost 100% in faint galaxies. For the brighter bins these fractions are much smaller than the values obtained from a direct naive average of the  $B/T$  histograms of Figure 12 because of the systematic effect we have just been discussing.

The error bars on the points in Figure 13 are important because they determine the precision of our final results. We neglect the formal errors on  $B/T$  returned by **Gim2D** because these are quite small, typically  $\pm 7\%$ , and are well below the systematic error discussed above due to the assignment of isophote twists or axial ratio changes to spurious thin disks. We assume, however, that this systematic can be neglected for systems with  $b/a < 0.5$ . The uncertainty in our estimate of the disk light fraction in each bin is then dominated by sampling. As a statistical model for the population of a particular bin we assume that a randomly chosen galaxy has a detectable edge-on disk ( $b/a < 0.5$ ) with probability  $p_{eo}$  where *a priori* we have  $0 < p_{eo} < 0.5$ . We also assume that the  $B/T$  values of these edge-on systems are drawn at random from some unknown distribution with population mean and variance which we estimate using the sample mean and variance,  $\langle B/T \rangle$  and  $\text{Var}(B/T)$  respectively. If the bin contains  $N_t$  galaxies of which  $N_{eo}$  have disks with  $b/a < 0.5$ , then the maximum likelihood estimate of  $p_{eo}$  is  $\tilde{p}_{eo} = N_{eo}/N_t$  provided  $N_{eo}/N_t < 0.5$  (it is equal to 0.5 otherwise). To approximate the variance of  $\tilde{p}_{eo}$  we use the standard binomial formula  $\text{Var}(\tilde{p}_{eo}) = \tilde{p}_{eo}(1 - \tilde{p}_{eo})/N_t$ , even though this is formally incorrect for  $\tilde{p}_{eo} \sim 0.5$ . Our estimate of the mean light fraction in edge-on disks is then  $(1 - \langle B/T \rangle)\tilde{p}_{eo}$  and we calculate the variance in this estimate as  $(\tilde{p}_{eo})^2 \text{Var}(B/T) + \langle B/T \rangle^2 \text{Var}(\tilde{p}_{eo})$ . These give the final results plotted when multiplied by the correction factor of equation 7 which accounts for the light in face-on disks. There is undoubtedly a systematic uncertainty associated with this last step, but we ignore it here.

We can now average the disk light fractions of Figure 13 over the galaxy population as whole in order to obtain the fractions of the total luminosity density in the local universe coming from disks and from bulges. The contribution of each of our absolute magnitude bins to the total luminosity density  $\Phi_{tot, k}$  can be obtained by integrating the appropriate Blanton et al. (2003) luminosity function across the bin. The final result for the fraction of the local luminosity

density in disks is then,

$$f_{disk} = \frac{\sum_k \Phi_{tot, k} \cdot f_{disk, k}}{\sum_k \Phi_{tot, k}}. \quad (9)$$

Note that the luminosity functions for our sample are quite consistent with those given by Blanton et al. (2003). We prefer to use the latter here because of their much better statistical precision. The final result we obtain for the total fraction of the light coming from disks in the local universe is  $(54 \pm 2)\%$ , with no detected dependence on observing band or decomposition parametrisation. The details are in Table 3. The error bars in this table are calculated directly from those in Figure 13 assuming the uncertainties in the different absolute magnitude bins to be independent. Uncertainties coming from the luminosity function itself are negligible in comparison.

A slight variation of this analysis allows us to calculate a second interesting quantity: the fraction of galaxies in each of our absolute magnitude bins which contain no detectable thin disk and so may be considered “pure” bulge systems. Our hypothesis here is that **Gim2D** will detect any significant disk if it is sufficiently inclined to the line-of-sight that  $b/a < 0.5$ . Exactly one half of all disk galaxies should be at least this inclined. We can thus estimate the number of effectively diskless galaxies in each bin by subtracting twice the number of objects with  $b/a$  estimates below 0.5 from the total number of galaxies in the bin. The result of this exercise is shown in Figure 14 in similar format to Figure 13. Again the results are very similar in the two pass-bands and for our two assumptions about bulge profiles. For the brightest bins we find that the great majority of galaxies are effectively diskless, while in the faintest bins our statistics are consistent with at most a small fraction of “pure bulge” systems. The fraction of “pure bulges” varies smoothly with absolute magnitude between these two extremes. The error bars reflect the binomial uncertainty in our estimate  $\tilde{p}_{eo} = N_{eo}/N_t$  of the fraction of the bin population with detectable edge-on disks.

As before we can combine the results of Figure 14 with the luminosity functions of Blanton et al. (2003) to estimate the fraction of the luminosity density of the local Universe which is contributed by effectively diskless systems. The result, given in detail in Table 4, is about  $(32 \pm 1)\%$  with no significant dependence on pass-band or bulge fitting function. Thus the breakdown of stellar luminosity in the local Universe is apparently 54% in disks, 32% in “pure bulge” systems with no photometrically detectable (by **Gim2d**) disk and only 14% in the bulges of galaxies with detectable disks.

## 6 CONCLUSIONS

We have used the two-dimensional photometric fitting programme **Gim2D** of Simard et al. (2002) on the images of an apparent magnitude limited sample of 1862 large galaxies selected from the SDSS and visually classified by Nakamura et al. (2003). In almost all cases the code returns a well-defined decomposition of the galaxy into disk and bulge components with parameters which have small formal error bars and vary little either between the  $r$  and  $i$  band images analysed here or between decompositions in which

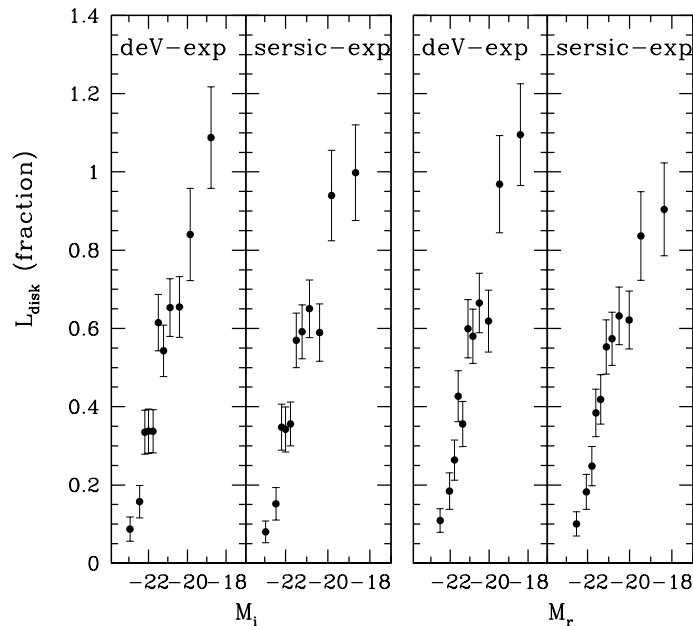


**Figure 13.** The two left-hand panels show the luminosity fraction in disks for galaxies in the Sloan  $i$  band. The galaxies are modelled with two different sets of parametric functions: a de Vaucouleurs profile for the bulge and an exponential for the disk (left panel) or a Sérsic profile for the bulge plus an exponential for the disk (right panel). The two right-hand panels show the same results but in the  $r$  band.

the Sérsic index of the bulge component varies or is fixed to the de Vaucouleurs value  $n = 4$ . The total amount of light in differences between the observed image and the best fit model is typically only about 10% of the galaxy luminosity. Despite this apparent success, we show that for intrinsically bright galaxies the “disk” component does not in most cases represent a true thin axisymmetric disk, since the sample distribution of axial ratios  $b/a$  deviates strongly from the uniform distribution expected for a population of such disks – near edge-on disks are grossly underrepresented. This problem was already noted by Simard et al. (2002). Apparently the code is using the degrees of freedom provided by the assumed disk component to fit radial changes in isophote shape or position angle within galaxies which have no real thin disk.

We attempt to correct for this systematic problem by concentrating on galaxies for which **Gim2D** finds a disk axial ratio  $b/a < 0.5$ . We argue that ellipsoidal stellar systems with such extreme apparent axial ratios are quite rare so that the component isolated by the decomposition programme is likely to be a highly inclined disk. Since the selection criteria for our sample depend at most weakly on inclination, we can use the assumption that our galaxy sample is randomly oriented to correct from the sample with highly inclined disks to the sample as a whole. Such corrections are at best approximate, since there are undoubtedly cases where the decomposition mixes light from the true bulge and disk components in such a way that photomet-

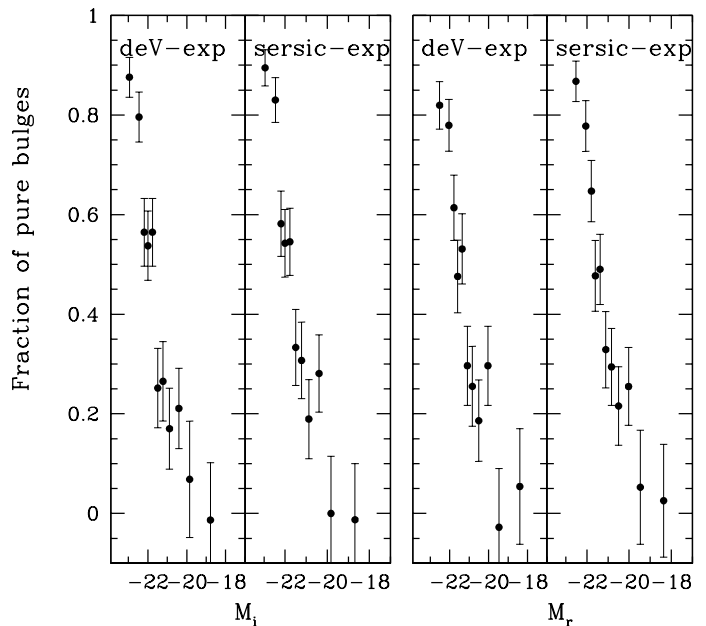


**Figure 14.** The two left-hand panels show the fraction of pure bulge galaxies as a function of the  $i$  band absolute magnitude. Different parametric functions are considered: de Vaucouleurs plus exponential (left-panel) and Sérsic plus exponential (right-panel). The two right-hand panels show the same results but in the  $r$  band.

rically fit “disk” has  $b/a > 0.5$  even though the galaxy is sufficiently inclined for the projected image of its true disk to have  $b/a < 0.5$ . Without further information (for example, from kinematics) it is very difficult to assess the size of the biases this may introduce.

As a first application we estimate average disk light fractions for galaxies as a function of absolute magnitude. These range from about 10% for the brightest galaxies to almost 100% for the faintest ones. At each absolute magnitude we also estimate the fraction of “pure bulge” galaxies, defined as galaxies for which **Gim2D** would detect no disk with  $b/a < 0.5$  even if the orientation were such that  $b/a < 0.5$  would be expected for any true axisymmetric thin disk. We find that most of the galaxies in the brighter absolute magnitude bins are “pure bulge” by this definition, but that this fraction decreases steadily for fainter systems. We do not detect any population of “pure bulges” in our faintest bin. These numbers differ substantially from those inferred naively from the  $B/T$  distributions measured directly by **Gim2D**: for example, in the brightest absolute magnitude bin about 85% of galaxies are “pure bulge” and disks only contribute  $\sim 10\%$  of the total light, yet the median value of  $B/T$  returned by the code is 0.55 and very few galaxies are fitted with  $B/T > 0.8$ .

By combining these results for the absolute magnitude dependence of the mean light fractions in disks or in “pure bulges” with the luminosity functions of Blanton et al. (2003), we have been able to estimate the fractions of all galaxy light in the local Universe coming from disks and

from “pure bulges”. The results depend little on the waveband used or on the bulge luminosity profile we adopt. We find that  $54 \pm 2\%$  of the local luminosity density is contributed by stars in disks and  $32 \pm 2\%$  by stars in “pure bulges”. The remaining  $14 \pm 3\%$  comes from bulges in systems with detectable disks. The mean bulge-to-total ratio of the latter systems is thus  $14/68 \sim 0.2$ , substantially smaller than typical  $B/T$  values in the histograms of Figure 12. Note that only sampling uncertainties are taken into account in the errors quoted here. Residual systematics may remain, reflecting the fact that real galaxies have a more complex structure than the models we use to describe them here. A fully convincing decomposition of galaxies into bulge and disk components clearly cannot be performed using imaging data alone. We believe, however, that the analysis of this paper provides the best quantitative indication so far of the overall distribution of stars between the two basic structural forms which make up galaxies.

## ACKNOWLEDGMENTS

We thank Luc Simard for help in using his excellent two-dimensional fitting package **Gim2D**. Funding for the creation and distribution of the SDSS Archive has been provided by the Alfred P. Sloan Foundation, the Participating Institutions, the National Aeronautics and Space Administration, the National Science Foundation, the U.S. Department of Energy, the Japanese Monbukagakusho, and the Max Planck Society. The SDSS Web site is <http://www.sdss.org/>.

The SDSS is managed by the Astrophysical Research Consortium (ARC) for the Participating Institutions. The Participating Institutions are The University of Chicago, Fermilab, the Institute for Advanced Study, the Japan Participation Group, The Johns Hopkins University, the Korean Scientist Group, Los Alamos National Laboratory, the Max-Planck-Institute for Astronomy (MPIA), the Max-Planck-Institute for Astrophysics (MPA), New Mexico State University, University of Pittsburgh, University of Portsmouth, Princeton University, the United States Naval Observatory, and the University of Washington.

## REFERENCES

Andredakis Y. C., 1998, MNRAS, 295, 725  
 Bertin E., Arnouts S., 1996, A&AS, 117, 393  
 Blanton M. R., Brinkmann J., Csabai I., Doi M., Eisenstein D., Fukugita M., Gunn J. E., Hogg D. W., Schlegel D. J., 2003, AJ, 125, 2348  
 Blanton M. R., Hogg D. W., Bahcall N. A., 2003, ApJ, 592, 819  
 Blanton M. R., Lin H., Lupton R. H., Maley F. M., Young N., Zehavi I., Loveday J., 2003, AJ, 125, 2276  
 Ciotti L., 1991, A&A, 249, 99  
 Courteau S., de Jong R. S., Broeils A. H., 1996, ApJ, 457, L73+  
 de Jong R. S., 1996, A&AS, 118, 557  
 de Vaucouleurs G., de Vaucouleurs A., Corwin H. G., Buta R. J., Paturel G., Fouque P., 1991, Third Reference Cat-

alogue of Bright Galaxies. Volume 1-3, XII, 2069 pp. 7 figs.. Springer-Verlag Berlin Heidelberg New York  
 Dressler A., 1980, ApJ, 236, 351  
 Efsthathiou G., Lake G., Negroponte J., 1982, MNRAS, 199, 1069  
 Eisenstein D. J., Annis J., Gunn J. E., Szalay A. S., Connolly A. J., Nichol R. C., Bahcall N. A., Bernardi M., Burles S., Castander F. J., 2001, AJ, 122, 2267  
 Fukugita M., Ichikawa T., Gunn J. E., Doi M., Shimasaku K., Schneider D. P., 1996, AJ, 111, 1748  
 Fukugita M., Nakamura O., Turner E. L., Helmboldt J., Nichol R. C., 2004, ApJ, 601, L127  
 Gunn J. E., Carr M., Rockosi C., Sekiguchi M., Berry K., Elms B., de Haas E., Ivezić Ž., 1998, AJ, 116, 3040  
 Hogg D. W., Finkbeiner D. P., Schlegel D. J., Gunn J. E., 2001, AJ, 122, 2129  
 Ivezić Ž., Lupton R. H., Schlegel D., Boroski B., Adelman-McCarthy J., Yanny B., Kent S., Stoughton C., Finkbeiner D., 2004, Astronomische Nachrichten, 325, 583  
 Kauffmann G., White S. D. M., Heckman T. M., Ménard B., Brinchmann J., Charlot S., Tremonti C., Brinkmann J., 2004, MNRAS, 353, 713  
 Kelly B. C., McKay T. A., 2004, AJ, 127, 625  
 Lupton R. H., Gunn J. E., Ivezić Z., Knapp G. R., Kent S., Yasuda N., 2001, in ASP Conf. Ser. 238: Astronomical Data Analysis Software and Systems X The SDSS Imaging Pipelines. pp 269–+  
 Lupton R. H., Ivezić Z., Gunn J. E., Knapp G., Strauss M. A., Yasuda N., 2002, in Survey and Other Telescope Technologies and Discoveries. Edited by Tyson, J. Anthony; Wolff, Sidney. Proceedings of the SPIE, Volume 4836, pp. 350-356 (2002). SDSS Imaging Pipelines. pp 350–356  
 Nakamura O., Fukugita M., Brinkmann J., Schneider D. P., 2004, AJ, 127, 2511  
 Nakamura O., Fukugita M., Yasuda N., Loveday J., Brinkmann J., Schneider D. P., Shimasaku K., SubbaRao M., 2003, AJ, 125, 1682  
 Pier J. R., Munn J. A., Hindsley R. B., Hennessy G. S., Kent S. M., Lupton R. H., Ivezić Ž., 2003, AJ, 125, 1559  
 Sandage A., 1961, The Hubble atlas of galaxies. Washington: Carnegie Institution, 1961  
 Schechter P. L., Dressler A., 1987, AJ, 94, 563  
 Schlegel D. J., Finkbeiner D. P., Davis M., 1998, ApJ, 500, 525  
 Sersic J. L., 1968, Atlas de galaxias australes. Cordoba, Argentina: Observatorio Astronomico, 1968  
 Simard L., Willmer C. N. A., Vogt N. P., Sarajedini V. L., Phillips A. C., Weiner B. J., Koo D. C., Im M., Illingworth G. D., Faber S. M., 2002, ApJS, 142, 1  
 Simion F., de Vaucouleurs G., 1986, ApJ, 302, 564  
 Smith J. A., Tucker D. L., Kent S., Richmond M. W., Fukugita M., Ichikawa T., 2002, AJ, 123, 2121  
 Stoughton C., Lupton R. H., Bernardi M., Blanton M. R., Burles S., Castander F. J., Connolly A. J., Eisenstein D. J., Frieman J. A., Hennessy G. S., Hindsley R. B., Ivezić Ž., Kent S., Kunszt P. Z., Lee B. C., Meiksin A., Munn J. A., 2002, AJ, 123, 485  
 Strauss M. A., Weinberg D. H., Lupton R. H., Narayanan V. K., Annis J., Bernardi M., Blanton M., Burles S., Connolly A. J., Dalcanton J., 2002, AJ, 124, 1810  
 York D. G., Adelman J., Anderson J. E., Anderson S. F.,

Annis J., Bahcall N. A., Bakken J. A., Barkhouser R., Bastian S., Berman E., Boroski W. N., Bracker S., Briegel C., Briggs J. W., Brinkmann J., Brunner R., 2000, *AJ*, 120, 1579